RESEARCH ARTICLE
ATMOSPHERIC PHYSICS

Earth and Planetary Physics
7: 665–674, 2023
doi: 10.26464/epp2023083

Mesopause temperatures and relative densities at midlatitudes observed by the Mengcheng meteor radar

Wen Yi[1,2], XiangHui Xue[1,2,3,4,5*], MaoLin Lu[1,2], Jie Zeng[1,2], HaiLun Ye[1,2], JianFei Wu[1,2], Chong Wang[1,2], and TingDi Chen[1,2]

[1]Chinese Academy of Sciences Key Laboratory of Geospace Environment, Department of Geophysics and Planetary Sciences, University of Science and Technology of China, Hefei 230026, China;

[2]Mengcheng National Geophysical Observatory, School of Earth and Space Sciences, University of Science and Technology of China, Hefei 230026, China;

[3]Hefei National Laboratory for the Physical Sciences at the Microscale, University of Science and Technology of China, Hefei 230026, China;

[4]Chinese Academy of Sciences Center for Excellence in Comparative Planetology, Hefei 230026, China;

[5]Collaborative Innovation Center of Astronautical Science and Technology, Harbin 150001, China

Key Points:

- In this study, we present more than 9 years of observations of mesopause temperatures and densities.
- Mesopause density (temperature) exhibits a seasonal structure similar to that of the zonal (meridional) wind.
- Meteor radar provides multiple mesospheric parameters for investigating mesospheric dynamics and thermodynamic processes.

Citation: Yi, W., Xue, X. H., Lu, M. L., Zeng, J., Ye, H. L., Wu, J. F., Wang, C., and Chen, T. D. (2023). Mesopause temperatures and relative densities at midlatitudes observed by the Mengcheng meteor radar. *Earth Planet. Phys.*, *7*(6), 665–674. http://doi.org/10.26464/epp2023083

Abstract: The atmospheric temperatures and densities in the mesosphere and lower thermosphere (MLT) region are essential for studying the dynamics and climate of the middle and upper atmosphere. In this study, we present more than 9 years of mesopause temperatures and relative densities estimated by using ambipolar diffusion coefficient measurements observed by the Mengcheng meteor radar (33.4°N, 116.5°E). The intercomparison between the meteor radar and Thermosphere Ionosphere Mesosphere Energetics and Dynamics/Sounding of the Atmosphere by Broadband Emission Radiometry (TIMED/SABER) and Earth Observing System (EOS) Aura/Microwave Limb Sounder (MLS) observations indicates that the meteor radar temperatures and densities agree well with the simultaneous satellite measurements. Annual variations dominate the mesopause temperatures, with the maximum during winter and the minimum during summer. The mesopause relative densities also show annual variations, with strong maxima near the spring equinox and weak maxima before the winter solstice, and with a minimum during summer. In addition, the mesopause density exhibits a structure similar to that of the zonal wind: as the zonal wind flows eastward (westward), the mesopause density decreases (increases). At the same time, the meridional wind shows a structure similar to that of the mesopause temperature: as the meridional wind shows northward (southward) enhancements, the mesopause temperature increases (decreases). Simultaneous horizontal wind, temperature, and density observations provide multiple mesospheric parameters for investigating mesospheric dynamics and thermodynamic processes and have the potential to improve widely used empirical atmospheric models.

Keywords: meteor radar; mesopause; horizontal wind; temperature; density

1. Introduction

The mesopause in summer is the coldest region of the Earth because gravity wave-driven mean meridional circulation results in upwelling and adiabatic cooling in the summer polar mesopause region (see, e.g., Fritts and Alexander, 2003). Accurate observations of mesopause temperature are essential for studying the short-term dynamics and long-term climate of the middle and upper atmosphere. However, the specific environment of the mesosphere makes obtaining continuous measurements of the mesopause temperature quite difficult. Ground-based radio radars, such as medium frequency and very high frequency radars, are widely used to measure the neutral horizontal wind in the mesosphere, but they are not capable of measuring neutral atmospheric temperatures and densities. Ground-based optical instruments, such as lidar and airglow spectrometers, can provide high temporal resolution and accurate temperature measurements but are limited to clear sky and often to nighttime conditions. Sounding rockets can provide good in situ soundings of neutral mesospheric temperatures, but the high cost and complicated logistics of launching rockets generally make them impractical for routine

First author: W. Yi, yiwen@ustc.edu.cn
Correspondence to: X. H. Xue, xuexh@ustc.edu.cn
Received 03 JUL 2023; Accepted 08 SEP 2023.
First Published online 11 OCT 2023.

observations.

For decades, meteor radars have been widely used for investigating the mesosphere and lower thermosphere (MLT) region, especially for investigating the neutral wind of the MLT region. Because of the advantages of continuous meteor radar measurements, meteor radar observations are widely used in detecting the dynamics and climate of the MLT region (Hall et al., 2012; Stober et al., 2012, 2014; Holmen et al., 2016; Batubara et al., 2018; Yi W et al., 2019a). In addition to wind monitoring, meteor radars can be used to derive the neutral atmospheric temperature (Hocking et al., 1997; Hocking, 1999; Hall et al., 2006; Holdsworth et al., 2006; Yi W et al., 2014, 2016; Holmen et al., 2016; Lee et al., 2016; Liu LB et al., 2017b; Kam et al., 2019), pressure (Nielsen et al., 2001; Kumar, 2007), and density (Takahashi et al., 2002; Younger et al., 2015; Reid et al., 2017; Yi W et al., 2017, 2018, 2019b).

In this study, we use the ambipolar diffusion coefficients derived from the University of Science and Technology of China's Mengcheng meteor radar (33.4°N, 116.5°E) to examine the mesopause temperature and relative density and to investigate the climatology of the mesopause temperature and relative density. In addition, we present an intercomparison between the meteor radar and observations by the Thermosphere Ionosphere Mesosphere Energetics and Dynamics/Sounding of the Atmosphere by Broadband Emission Radiometry (TIMED/SABER) and Earth Observing System (EOS) Aura/Microwave Limb Sounder (MLS). This article is organized as follows. In Section 2, we introduce the experimental instruments and their datasets. Then, in Sections 3 and 4, we present the mesopause temperatures and relative densities at midlatitudes derived by the Mengcheng meteor radar. Finally, we summarize our results.

2. Data and Methods

The Mengcheng all-sky interferometric meteor radar (MCMR) was installed at the midlatitude station in Mengcheng (33.36°N, 116.49°E), Anhui Province, and has been operated by the University of Science and Technology of China since April 2014. The MCMR belongs to the ATRAD Enhanced Meteor Detection Radar (EMDR) series and is essentially the same as that described by Holdsworth et al. (2004). As shown in Figure 1 and Table 1, the MCMR transmits a coherent-pulse radio signal at a frequency of 38.9 MHz corresponding to a wavelength (λ) of 7.71 m and a peak power of 20 kW. The MCMR uses a 4-bit code and a pulse repetition frequency of 430 Hz with four sample integrations.

Figure 2a shows the daily number of meteors observed by the MCMR. The MCMR typically detects approximately 6000–20,000 underdense meteor echoes per day, which is enough to estimate the daily temperature and density. The number of meteors per hour observed by the MCMR is approximately 200–1600, which is enough to provide a horizontal wind field at an altitude of 76 to 100 km. The seasonal variations in the meteor count rates observed by the MCMR (at midlatitudes in the Northern Hemisphere) show a clear annual variation, with a maximum in September–October and a minimum in February. Measurements obtained by the MCMR from April 2014 to June 2022 are used in this study. Although some data gaps exist because of site maintenance, the MCMR data still have good continuity for investigating the atmospheric dynamics and climatology in the MLT region at midlatitudes. Figures 2b and 2c show the peak height and width of the detection distribution of meteor echoes observed by the MCMR.

In Figure 2b, the peak height observed by the MCMR shows annual variation, with a maximum value of approximately 92 km in winter and a minimum value of approximately 88.5 km in summer. The width of the meteor distribution fluctuates from 4.5 km in summer to 6.5 km in winter. The peak height of the meteor distribution can be used to indicate variations in mesospheric density, but it is also significantly affected by seasonal variations

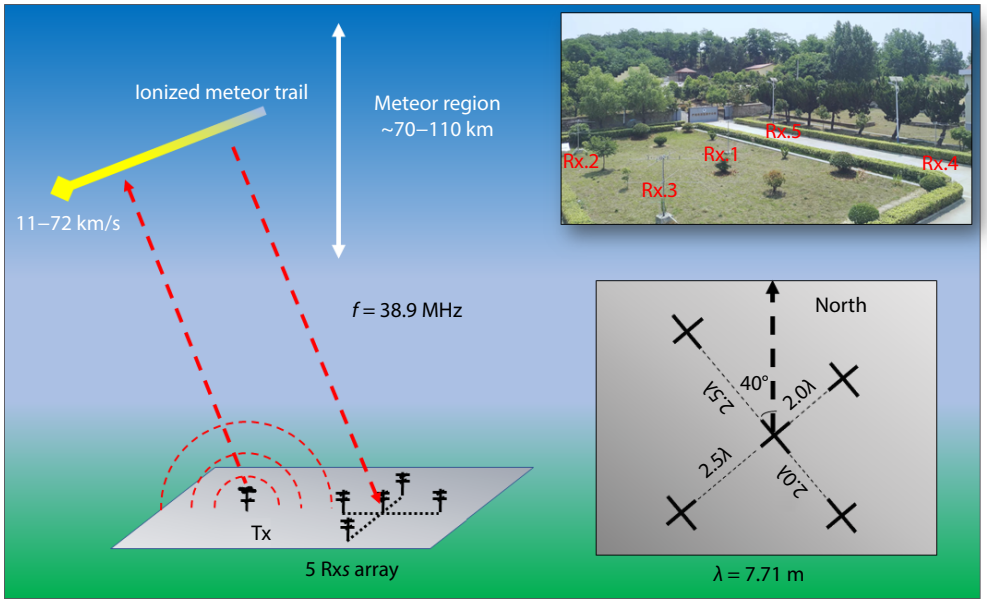

Figure 1. Schematic diagram of the geometry of the Mengcheng meteor radar. The bottom right inset shows the receiving array consisting of an arrangement of five two-element Yagi antennas. The upper right inset shows a picture of the Mengcheng meteor radar receiving antenna array.

Table 1. Main operating parameters of the Mengcheng meteor radar.

Frequency	38.9 MHz
Peak power for transmitter	24 kW
Pulse repetition frequency	430 Hz
Transmission mode	Circular
Coherent integrations	4
Range resolution	1.8 km
Pulse type	Gaussian
Pulse width	7.2 km

in meteor velocity (e.g., Yi W et al., 2017, 2018). The peak height at Davis Station (68.6°S) in the Antarctic mainly shows annual variation, reaching its maximum in summer (January) and minimum in winter (July). Similarly, the meteor radars located at the Arctic stations of Svalbard (78.3°N) and Tromsø (69.6°N) display peak heights that primarily follow an annual variation with an additional semiannual variation. The maximum peak height occurs in autumn (October), whereas the minimum height is observed in spring (February). The peak altitude at Mohe, China (53.5°N), at higher northern midlatitudes, indicates a semiannual oscillation and a relatively weak annual oscillation. At northern midlatitudes, the peak height in Beijing, China (40.3°N), mainly exhibits annual variations, with the maximum peak height recorded in autumn (October–November) and the minimum during summer (July; e.g., Liu LB et al., 2017a; Yi W et al., 2021).

2.1 TIMED/SABER and EOS Aura/MLS

The SABER instrument is carried onboard the TIMED satellite, which was launched in December 2001. The SABER measures CO_2 infrared limb radiance from the tropopause to the lower thermosphere, and kinetic temperature profiles are retrieved over these altitudes by using a full non-local thermodynamic equilibrium (LTE) inversion (Xu JY et al., 2006; Remsberg et al., 2008).

The MLS instrument is onboard the EOS Aura spacecraft, which was launched in 2004. The MLS observes atmospheric thermal microwave emissions in five spectral regions from 115 GHz to 2.5 THz. Temperatures are retrieved from bands near the O_2 spectral lines at 118 and 239 GHz detected by the MLS radiometers (Schwartz et al., 2008).

The temperature and density obtained from the SABER profiles (version 2.0) and the temperature and geopotential height obtained from the MLS profiles (version 4.2) were selected from a 5° × 20° grid in latitude and longitude centered on the Mengcheng meteor radar location, and the daily mean satellite

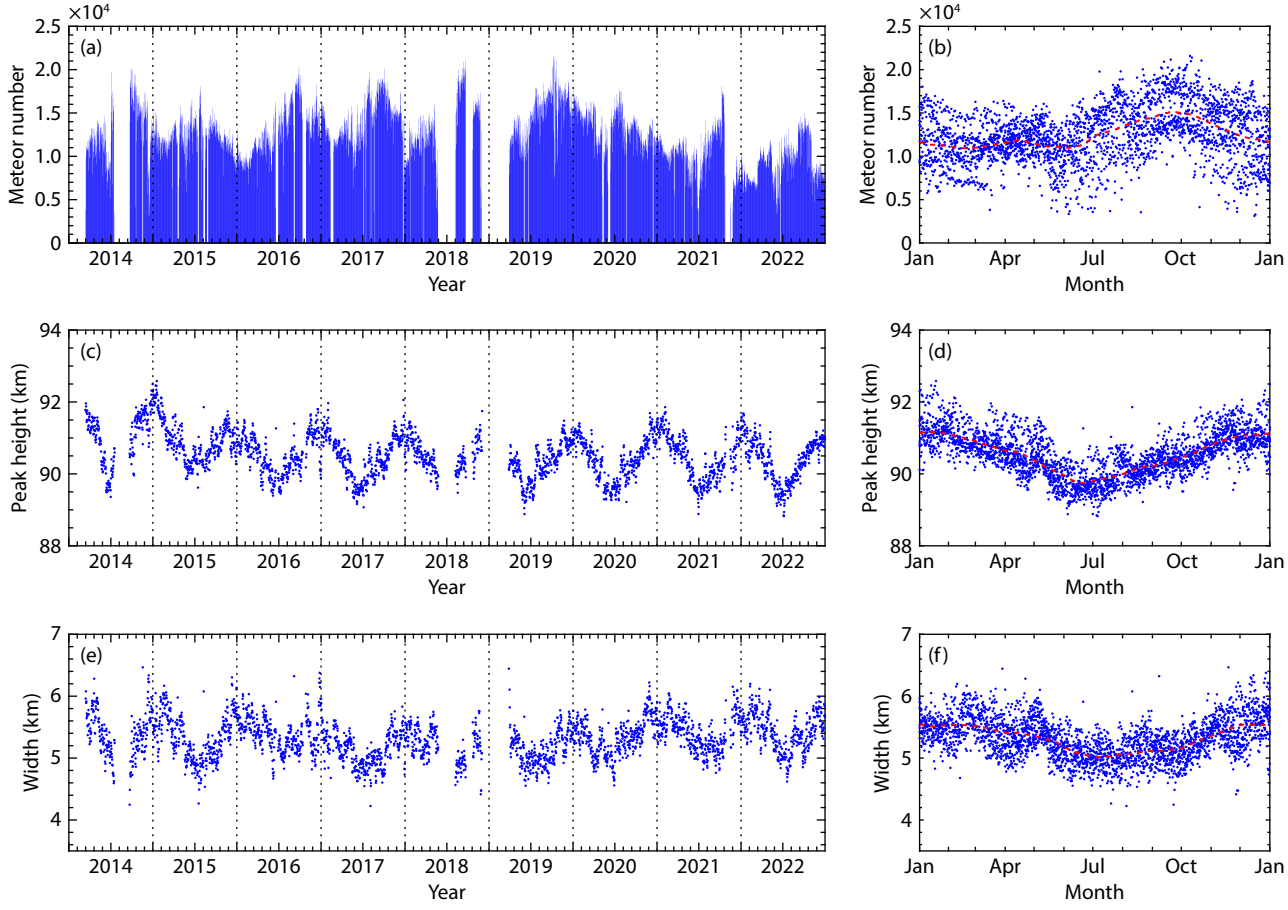

Figure 2. (a) Meteor count rate, (b) peak height, and (c) width of the meteor detection distribution from 2014 to 2022 observed by the Mengcheng meteor radar. Scatterplot of the composite (d) meteor count rate, (e) peak height, and (f) width of the meteor detection distribution as a function of the day of the year. The red dotted lines represent the 30-day running mean values.

temperatures and densities were averaged from these satellite measurements.

3. Mesopause Temperature Estimation Using the Mengcheng Meteor Radar

The ambipolar diffusion coefficient, D_a, of the plasma in an underdense meteor trail can be derived from the meteor radar echo decay time from the relation (e.g., Chilson et al., 1996; Hocking et al., 1997)

$$D_a = \frac{\lambda^2}{16\pi^2\tau}, \tag{1}$$

where λ is the wavelength of the meteor radar and τ is the time taken for the echo power to decay by a factor of e^{-2} of the initial maximum value. Measurements of ambipolar diffusion coefficients (D_a) observed by meteor radar can be used to estimate atmospheric temperature and pressure according to the relationship $D_a \propto T^2/P$ (Hocking et al., 1997; Cervera and Reid, 2000). In this study, we estimate the mesopause neutral temperature by using the ambipolar diffusion gradient method from meteor radar as follows. An expression for temperature is given by Hocking (1999), and a more detailed description of this technique can be found in Yi W et al. (2016):

$$T = S\left(2\frac{\mathrm{d}T}{\mathrm{d}z} + \frac{mg}{k}\right)\log_{10}\mathrm{e}, \tag{2}$$

where T is the temperature at peak height (as shown in Figure 2b), S is the slope of $\log_{10}D_a$ as a function of height, and D_a is the ambipolar diffusion coefficient. The expression $\mathrm{d}T/\mathrm{d}z$ is the vertical temperature gradient, which we model by averaging the Aura MLS temperature measurements. Variable m is the mass of a typical atmospheric particle, g is the gravitational acceleration at the meteor peak height (g = 9.49 m/s^2 at 90 km altitude), and k is the Boltzmann constant (Hocking, 1999). The approach to the estimation of slope S has been described in detail by Yi W et al. (2016, 2021, and references therein); therefore, we present only the results here.

Figure 3 shows the results of the northern midlatitude mesopause temperature estimated by using the MCMR measurements. In Figure 3a, the temperature gradient ($\mathrm{d}T/\mathrm{d}z$) models used in this study are based on the Aura/MLS temperature gradient averaged from an altitude of 80 km (at a pressure level of 0.01 hPa) to an altitude of 88 km (at a pressure level of 0.0022 hPa) over the MCMR. The temperature gradient model is estimated by applying a harmonic fit of the annual, semiannual, terannual, and quarterly components. The estimated gradient models over the MCMR at northern midlatitudes mainly show annual and semiannual variations, with a maximum in autumn and spring and a minimum in summer. As shown above, we calculated the slope S and formed a temperature gradient model. However, in general, the temperatures derived from meteor radar using the ambipolar diffusion gradient method show larger fluctuations than do the actual temperatures (Holdsworth et al., 2006; Yi W et al., 2016).

As shown in Figure 3b, we illustrate the calibration of the MCMR temperatures by using the simultaneous MLS temperatures. Figure 3b shows a scatterplot of 2682 simultaneous daily temperatures obtained from the MCMR and MLS, with a correlation coefficient of 0.78. The strong correlation between the MCMR and MLS temperatures indicates that the two independent measurements can accurately estimate the mesopause temperatures. However, to account for the different ranges in the temperature estimates, we use the MLS temperature to calibrate the meteor radar temperature. The red line shows the linear fitting between the MCMR and MLS temperatures. The fitted relationship is

$$T_{\mathrm{MLS}} = 0.39\,T_{\mathrm{MCMR}} + 109.1,$$

in units of kelvin (K). Figure 3c shows the differences in daily temperatures between the MCMR and the MLS and SABER measurements. This representation is similar to the analysis by Yi W et al. (2021). The mean differences between the MCMR and MLS temperatures are less than ±1 K. The lower biases of the MCMR temperature with respect to the SABER data become greater at −7.8 K. In the mesopause region, the SABER temperatures show a warm bias with respect to the MLS temperatures throughout most latitudes, with an approximately +5 K bias in the southern polar region and an approximately +10 K bias in low latitudes (Hoppel et al., 2008; Schwartz et al., 2008; Nguyen and Palo, 2013). A bias of approximately +7 K exists between the daily SABER and MLS temperature measurements over MCMR at midlatitudes, which can explain the lower biases of the MCMR temperatures with respect to the SABER data.

Figure 3d shows a comparison of the calibrated MCMR temperatures between the SABER and MLS temperatures. The calibrated MCMR temperatures show reasonable agreement with the SABER, with a correlation coefficient of 0.59 lower than the correlation coefficient of 0.78 between the MLS and MCMR temperatures. It should be noted that the correlation coefficient between the daily mean MLS and SABER temperatures is 0.61, which also explains the lower correlation between the MCMR and SABER temperatures. Figure 3e shows the monthly mean temperatures derived from the MCMR, SABER, and MLS measurements, and the mass spectrometer incoherent scatter (MSIS) model (NRLMSISE-00; Picone et al., 2002) over the MCMR. The MCMR, SABER, and MLS temperatures show the dominant annual variations, with a maximum during winter and a minimum during summer. The MSIS temperatures generally exhibit annual and weak semiannual variations, with a clear minimum during summer but a maximum (temperature warming) during autumn (October) and spring (April).

To better understand the seasonal variations in the mesopause temperatures at midlatitudes, in Figure 4 we show the results of harmonic fits for the MCMR temperatures. The MCMR temperatures mainly show annual variations. The largest of the annual variations has an amplitude of 8.3 K. It is interesting to note that the scatterplots of the composite temperatures show some intraseasonal variations at periods of 75 and 60 days and with amplitudes of 2.1 and 2.6 K. Tang YH et al. (2023) analyzed the intraseasonal oscillations (ISOs, 30–100 days) in the MLT region by using the horizontal wind observed by the MCMR and found a clear seasonal variation in ISOs in the horizontal wind at 80 km, which was strongest during the winter and weakest during the summer. Yi W et al. (2019a) reported evidence for oscillations near 90 days in mesospheric temperatures and winds observed by the Kunming

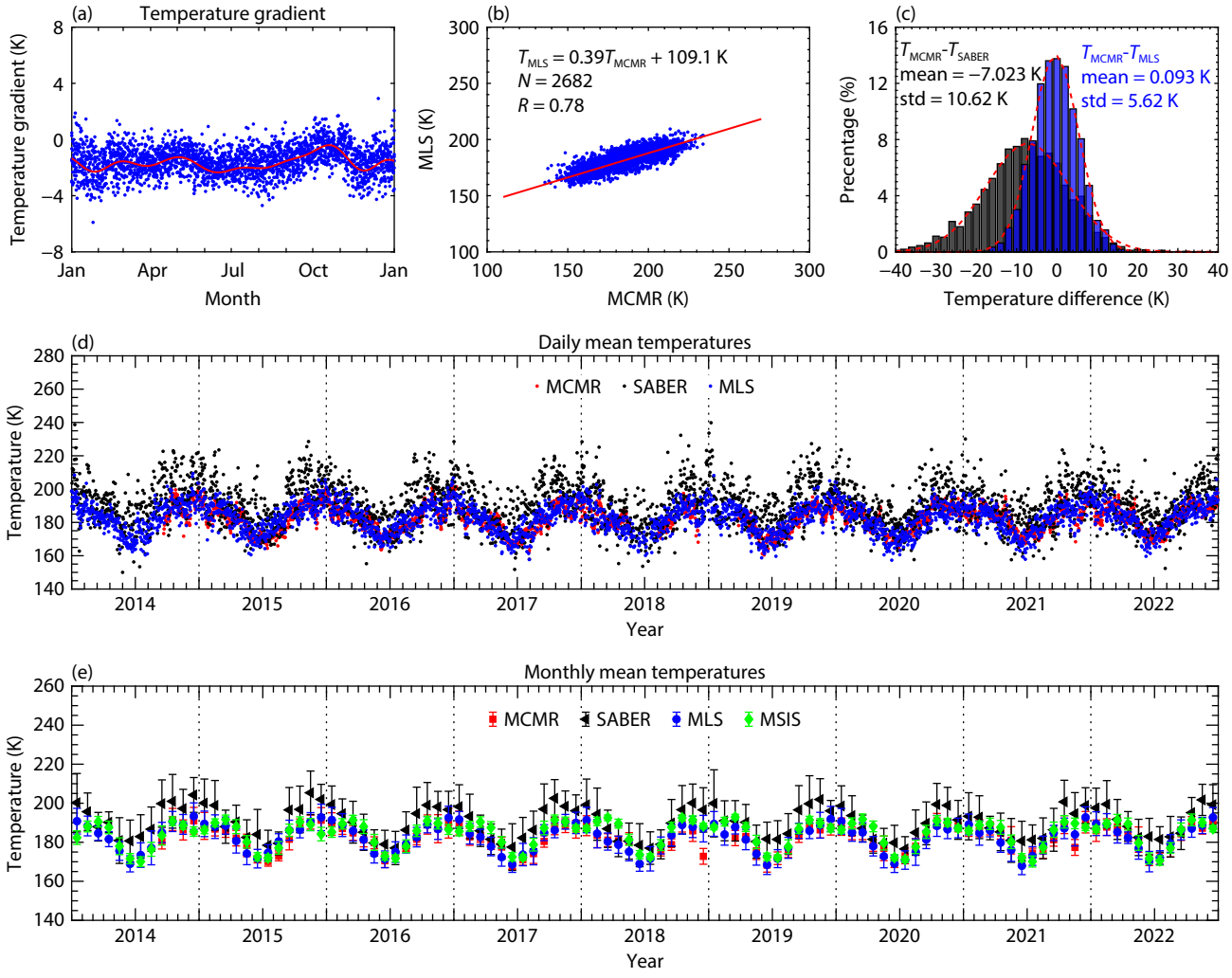

Figure 3. (a) The temperature gradient was calculated by averaging the Aura MLS temperatures from an altitude of 80 km (at a pressure level of 0.01 hPa) to an altitude of 88 km (at a pressure level of 0.0022 hPa) from 2014 to 2022 over the MCMR. The red solid line indicates the harmonic fit of the annual, semiannual, terannual, and quarterly components to create a temperature gradient model. (b) The linear fit of the MCMR and MLS temperatures, whose correlation coefficient is 0.78. The linear fitted expression for the relationship is $T_{MLS} = 0.39T_{MCMR} + 109.1$, in units of kelvin. (c) Histograms and Gaussian fits of temperature differences between the MCMR and MLS at a pressure level of 0.0022 hPa and SABER temperatures at 90 km. The means and standard deviations are shown for each fitted Gaussian distribution. (d) The calibrated daily mean MCMR temperatures are compared with the daily SABER and MLS temperatures. The correlation coefficients between the daily mean MCMR temperatures and the MLS and SABER temperatures are 0.78 and 0.59, respectively. (e) The monthly mean MCMR temperatures are compared with the monthly mean SABER, MLS, and MSIS (NRLMSISE-00) model temperatures.

meteor radar at lower latitudes (25.6°N); these variations mainly appeared in the winter and spring. Gong Y et al. (2022) analyzed the MLT horizontal winds observed by the Mohe meteor radar at higher midlatitudes (53.5°N) and reported that prominent ISOs with a period of 40–60 days appeared in the winter season and were likely associated with the equatorial Madden–Julian Oscillations in the troposphere. It is clear that ISOs in mesopause temperature observed by the MCMR mainly appear in the winter and spring, and these periodicity variations may be similar to the Madden–Julian Oscillations from the lower atmosphere (Eckermann and Vincent, 1994).

4. Mesopause Relative Density Estimation Using the Mengcheng Meteor Radar

The ambipolar diffusion coefficient D_a describes the rate at which plasma diffuses in a neutral background; it is a function of atmospheric temperature (T) and atmospheric pressure (P) or atmospheric density (ρ) (Hocking et al., 1997; Cervera and Reid, 2000), as given by

$$D_a = 6.39 \times 10^{-2} K_0 \frac{T^2}{P} = 2.23 \times 10^{-4} K_0 \frac{T}{\rho}, \quad (3)$$

where K_0 is the ion zero-field mobility factor. Following Chilson et al. (1996), Hocking et al. (1997), and Cervera and Reid (2000), we assumed K_0 to be $2.5 \times 10^{-4} \mathrm{m^{-2} s^{-1} V^{-1}}$. Given the relation in Equation (3), measurements of ambipolar diffusion can be used to retrieve the neutral mesospheric temperature by using the supplied value of pressure (Nielsen et al., 2001; Hall et al., 2012; Holmen et al., 2016) or to retrieve the pressure or density by using a predetermined temperature (Hocking et al., 1997; Takahashi

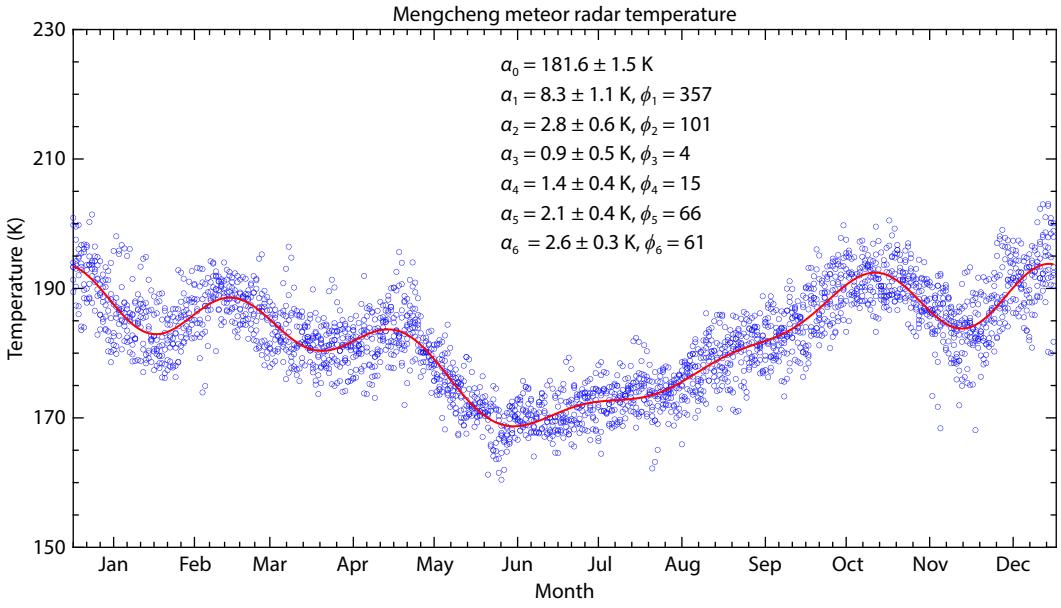

Figure 4. The yearly composite temperatures are estimated from the Mengcheng meteor radar. The red line represents the harmonic fitting with periodic 365/[1, 2, 3, 4 5, 6] components. The amplitudes and phases of the components are marked.

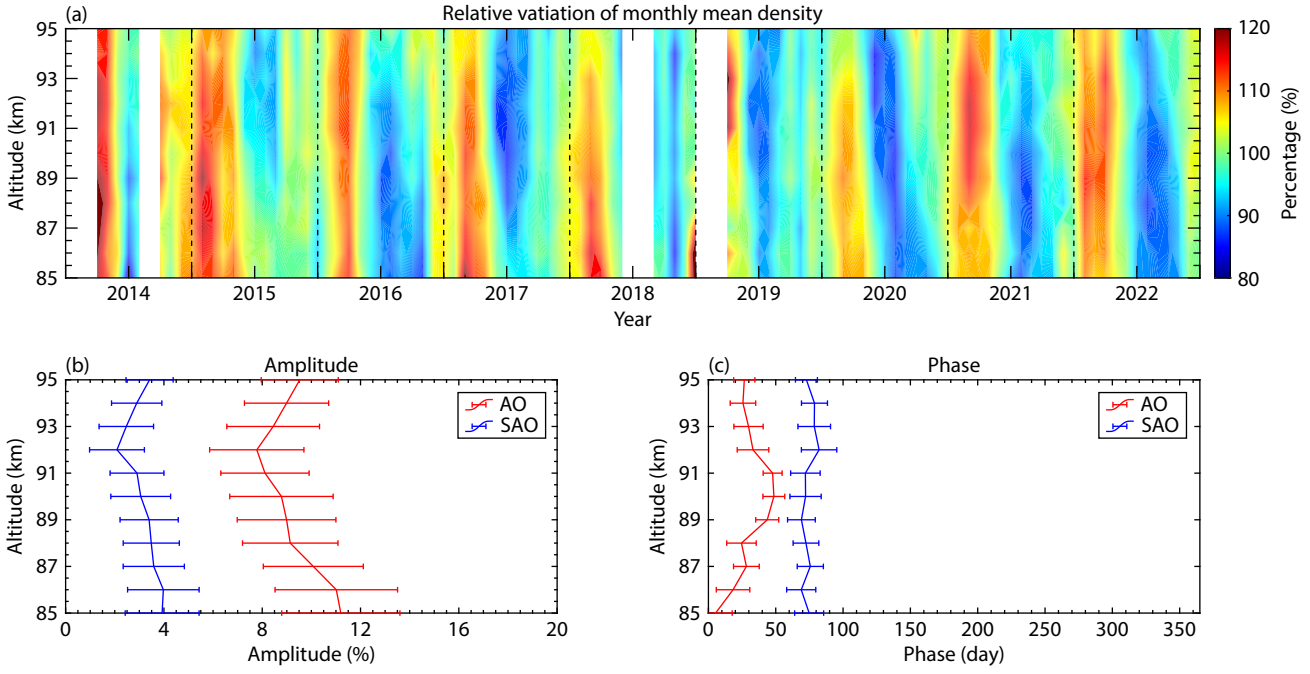

Figure 5. (a) Variations in the monthly mean relative densities at altitudes from 85 to 95 km were obtained from the Mengcheng meteor radar between 2014 and 2022. The color bars indicate the percentage variation in the monthly mean density relative to the mean density from the total observational time period. Amplitudes (b) and phases (c) of the annual oscillation (AO) and semiannual oscillation (SAO) observed by the Mengcheng meteor radar. The amplitude values indicate the percentage of the density relative to the mean density from the total observational time period.

et al., 2002).

Figure 5 shows the monthly mean mesospheric densities at northern midlatitudes derived from the MCMR. The MCMR monthly mean densities from April 2014 to December 2022 at lower midlatitudes in Figure 5a clearly show annual variations, with a clear minimum during summer and a maximum during spring. Figure 5b shows the amplitudes of the annual and semiannual variations. It is clear that the annual variations are much stronger than the semiannual variations. The amplitudes of the annual and semiannual variations reach 10% and 5% at 91 km and 85 km, respectively. The phases of the annual variation roughly show a decreasing trend as latitudes decrease and a downward progression as altitudes increase.

To better appreciate the seasonal variations in the mesopause

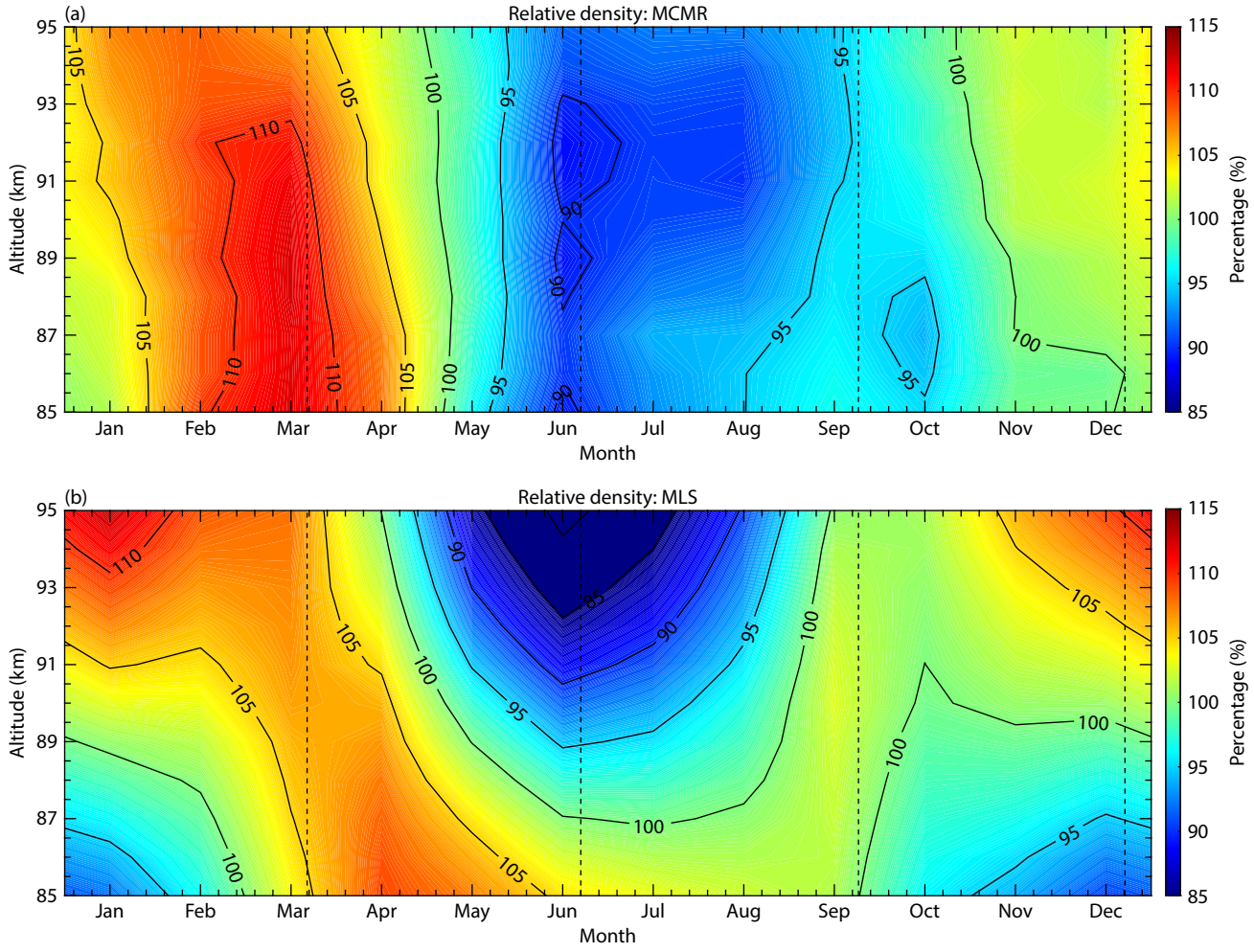

Figure 6. Contours of the composite monthly mean values of the mesopause relative densities obtained from the (a) Mengcheng meteor radar and (b) Aura/MLS in the composite year. The color bars indicate the percentage variation in mesopause density relative to the mean density from the total observational time period. The vertical black dashed lines depict the spring and autumn equinoxes and summer and winter solstices.

relative density, we show a composite analysis for the MCMR density in Figure 6a. The mesopause relative densities at midlatitudes show strong maxima near the spring equinox, weak maxima before the winter solstices, and minima in summer. As shown in Figure 6b, for comparison, we calculate the relative densities using the Aura/MLS measurements, and we use the calculation of the MLS temperature and geopotential height measurements in Younger et al. (2014). In general, the results of the comparison show that the MCMR densities have seasonal variations similar to those with the MLS measurements above 90 km. However, the MCMR densities show inconsistencies between the MLS densities below 90 km. These inconsistencies may be caused by the neutralization of meteoric plasma in addition to ambipolar diffusion (Lee et al., 2013; Younger et al., 2014).

In addition, in Figure 7, we show the composite seasonal variation in zonal and meridional winds from 2014 to 2022 observed by the MCMR (e.g., Yi W et al., 2023) compared with the mesopause relative densities obtained from MLS measurements and temperatures observed by SABER. It is interesting to note that the mesopause density (as shown in Figure 7c) exhibits a structure similar to that of the mesopause zonal wind (as shown in Figure 7a): as the zonal wind flows eastward, the mesopause density decreases, and vice versa. Yi W et al. (2019b) reported that the maxima of the yearly variations in the mesopause relative densities display a clear latitudinal variation across the spring equinox as the latitude decreases. Zhou BZ et al. (2022) also reported that the time of the maximum eastward zonal wind flows observed by meteor radars at different latitudes slowly shifts from summer to spring. These similar latitudinal variation characteristics between mesospheric density and zonal wind may be related to latitudinal changes influenced by gravity wave forcing. Zhou BZ et al. (2023) reported the simultaneous response of neutral density and horizontal wind observed by high- and midlatitude meteor radars to stratospheric sudden warmings (SSWs). Their results indicated that at high (middle) latitudes, the neutral density increased (decreased) at the beginning of SSW events and decreased (increased) after the zonal mean stratospheric temperature reached the maximum. At the same time, the zonal wind at high (middle) latitudes showed a westward (eastward) enhancement at the beginning of SSWs and then an eastward (westward) enhancement after the stratospheric temperature reached a maximum. These results show that an obvious relationship exists between the mesopause density and the zonal wind.

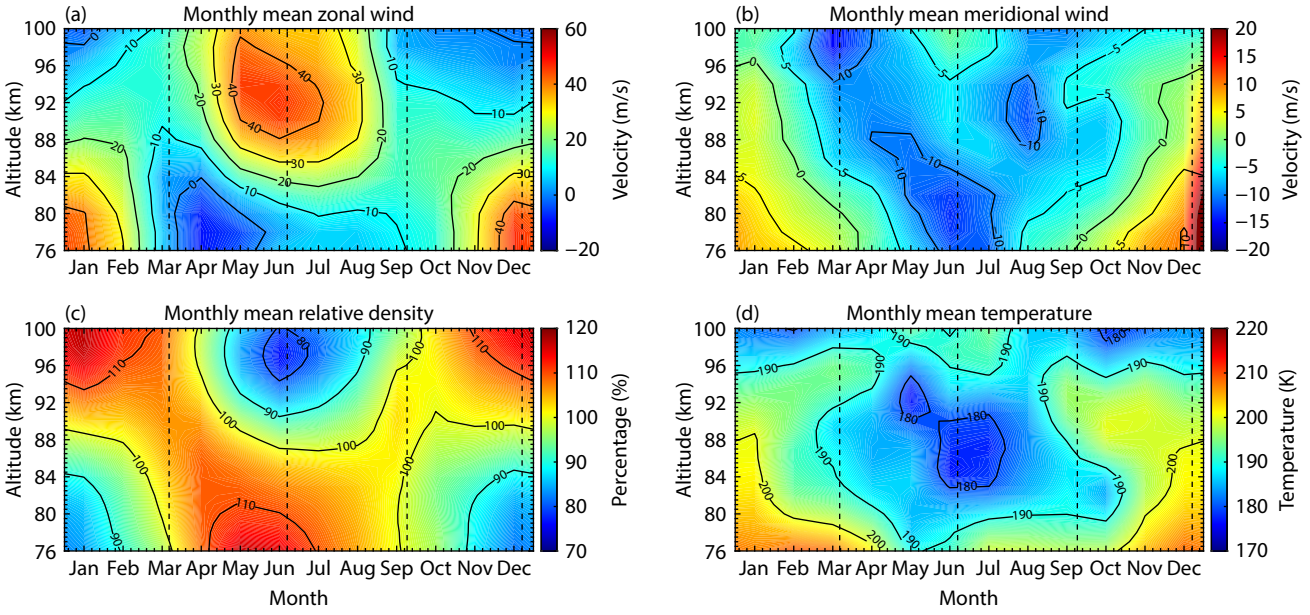

Figure 7. Composite of monthly mean (a) zonal (eastward is positive) and (b) meridional (northward is positive) winds from 2014 to 2022 observed by the Mengcheng meteor radar compared with the monthly mean (c) relative density obtained by the MLS measurements and (d) temperature obtained from the SABER measurements. The vertical black dashed lines depict the spring and autumn equinoxes and summer and winter solstices.

In Figures 7b and 7d, we also find that the mesopause meridional wind observed by the MCMR and mesopause temperature observed by the SABER show similar seasonal patterns. In general, as the meridional wind flow shows northward enhancements, the mesospheric temperature increases, and vice versa. The meridional winds mainly show annual variation, with a strong northward wind during winter and a southward wind during summer. At the same time, the mesopause temperatures also show annual variations, with a maximum during winter and a minimum during summer. This phenomenon typically represents the energy conversion between atmospheric dynamics and thermodynamics in the MLT region. The mesopause density and wind relationship is apparent for the zonal wind component but not for the meridional wind component, which may be related to the balance wind relationship. For example, the balance wind relationship is used to derive averaged zonal winds in the tropics from satellite retrievals of geopotential height (Smith et al., 2017). These remarkable relationships between the atmospheric wind, temperature, and density are very complex, and their mechanisms are not independent because these atmospheric parameters interact with each other; however, these are beyond the scope of this study at the moment and are the subject of ongoing work.

5. Summary and Conclusions

In this article, we have described an all-sky meteor radar system deployed at Mengcheng Station (33.4°N, 116.4°E). The radar system made nearly continuous measurements of winds in the mesosphere and lower thermosphere from April 2014 to the present, which has good continuity for investigating the atmospheric dynamics and climatology in the MLT region at midlatitudes. Here, we present more than 9 years of mesopause temperatures and relative densities over Mengcheng and compare our measurements with the SABER and Aura/MLS observations. The main points we found can be summarized as follows:

(1) Approximately 6000–20,000 underdense meteor echoes are observed per day by the Mengcheng meteor radar, which is sufficient for the estimation of daily temperature and relative density in the MLT region. The meteor count rates observed by the MCMR show a clear annual variation, with a maximum in September–October and a minimum in February.

(2) Mesopause temperatures were estimated by applying the ambipolar diffusion gradient method with data observed by the Mengcheng meteor radar. The temperature gradient model over Mengcheng was developed by using the Aura/MLS temperature. Linear calibration factors for the Mengcheng meteor radar temperature were obtained by using the Aura/MLS temperature. The calibrated temperatures estimated from meteor radars agree with the SABER and MLS temperatures. In northern midlatitudes, the annual variations dominate the seasonal variations in mesopause temperatures.

(3) Mesopause relative densities were estimated by applying the ambipolar diffusion and Aura/MLS temperatures. In northern midlatitudes, the mesopause relative densities from the MCMR show strong maxima near the spring equinox and weak maxima before the winter solstices. The minima of the mesopause relative densities basically appear during summer.

(4) The mesopause temperature, density, and horizontal wind can be obtained simultaneously by the MCMR meteor radar. The mesopause density observations show a seasonal structure similar to that of the zonal wind: as the zonal wind flows eastward (westward), the mesospheric density decreases (increases). At the same time, the mesopause temperature shows a structure similar to

that of the meridional wind: as the meridional wind shows northward enhancement, the mesopause temperature increases, and vice versa.

These results highlight the important contribution of MLT measurements made by the Mengcheng meteor radar, through which we can develop our understanding of MLT dynamics and climate. Long-term continuous observations of wind, temperature, and density can be used to guide further investigation of long-term trend changes in the MLT region, and they provide a wide range of opportunities to improve widely used atmospheric models.

Acknowledgments

This work is supported by the National Natural Science Foundation of China (Grant Nos. 42125402 and 42174183), the National Key Technologies R&D Program of China (Grant No. 2022YFF0503703), the B-type Strategic Priority Program of the Chinese Academy of Sciences (Grant No. XDB41000000), and the foundation of the National Key Laboratory of Electromagnetic Environment and the Fundamental Research Funds for the Central Universities, and the Chinese Meridian Project. WY is also funded by the Anhui Provincial Natural Science Foundation (Grant No. 2008085MD113) and the Joint Open Fund of Mengcheng National Geophysical Observatory (No. MENGO-202209). We acknowledge the technical support of our radar systems by Chris Adami.

References

Batubara, M., Yamamoto, M. Y., Madkour, W., and Manik, T. (2018). Long-term distribution of meteors in a solar cycle period observed by VHF meteor radars at near-equatorial latitudes. *J. Geophys. Res.: Space Phys.*, *123*(12), 10403–10415. https://doi.org/10.1029/2018JA025906

Cervera, M. A., and Reid, I. M. (2000). Comparison of atmospheric parameters derived from meteor observations with CIRA. *Radio Sci.*, *35*(3), 833–843. https://doi.org/10.1029/1999RS002226

Chilson, P. B., Czechowsky, P., and Schmidt, G. (1996). A comparison of ambipolar diffusion coefficients in meteor trains using VHF radar and UV lidar. *Geophys. Res. Lett.*, *23*(20), 2745–2748. https://doi.org/10.1029/96GL02577

Eckermann, S. D., and Vincent, R. A. (1994). First observations of intraseasonal oscillations in the equatorial mesosphere and lower thermosphere. *Geophys. Res. Lett.*, *21*(4), 265–268. https://doi.org/10.1029/93GL02835

Fritts, D. C., and Alexander, M. J. (2003). Gravity wave dynamics and effects in the middle atmosphere. *Rev. Geophys.*, *41*(1), 1003. https://doi.org/10.1029/2001RG000106

Gong, Y., Xue, J. W., Ma, Z., Zhang, S. D., Zhou, Q. H., Huang, C. M., Huang, K. M., and Li, G. Z. (2022). Observations of a strong intraseasonal oscillation in the MLT region during the 2015/2016 winter over Mohe, China. *J. Geophys. Res.: Space Phys.*, *127*(6), e2021JA030076. https://doi.org/10.1029/2021JA030076

Hall, C. M., Aso, T., Tsutsumi, M., Höffner, J., Sigernes, F., and Holdsworth, D. A. (2006). Neutral air temperatures at 90 km and 70°N and 78°N. *J. Geophys. Res.: Atmos.*, *111*(D14), D14105. https://doi.org/10.11029/12005JD006794

Hall, C. M., Dyrland, M. E., Tsutsumi, M., and Mulligan, F. J. (2012). Temperature trends at 90 km over Svalbard, Norway (78°N 16°E), seen in one decade of meteor radar observations. *J. Geophys. Res.: Atmos.*, *117*(D8), D08104. https://doi.org/10.1029/2011JD017028

Hocking, W. K., Thayaparan, T., and Jones, J. (1997). Meteor decay times and their use in determining a diagnostic mesospheric temperature–pressure parameter: Methodology and one year of data. *Geophys. Res. Lett.*, *24*(23), 2977–2980. https://doi.org/10.1029/97GL03048

Hocking, W. K. (1999). Temperatures using radar–meteor decay times. *Geophys. Res. Lett.*, *26*(21), 3297–3300. https://doi.org/10.1029/1999GL003618

Holdsworth, D. A., Reid, I. M., and Cervera, M. A. (2004). Buckland Park all-sky interferometric meteor radar. *Radio Sci.*, *39*(5), RS5009. https://doi.org/10.1029/2003RS003014

Holdsworth, D. A., Morris, R. J., Murphy, D. J., Reid, I. M., Burns, G. B., and French, W. J. R. (2006). Antarctic mesospheric temperature estimation using the Davis mesosphere–stratosphere–troposphere radar. *J. Geophys. Res.: Atmos.*, *111*(D5), D05108. https://doi.org/10.1029/2005JD006589

Holmen, S. E., Hall, C. M., and Tsutsumi, M. (2016). Neutral atmosphere temperature trends and variability at 90 km, 70°N, 19°E, 2003–2014. *Atmos. Chem. Phys.*, *16*(12), 7853–7866. https://doi.org/10.5194/acp-16-7853-2016

Hoppel, K. W., Baker, N. L., Coy, L., Eckermann, S. D., McCormack, J. P., Nedoluha, G. E., and Siskind, D. E. (2008). Assimilation of stratospheric and mesospheric temperatures from MLS and SABER into a global NWP model. *Atmos. Chem. Phys.*, *8*(20), 6103–6116. https://doi.org/10.5194/acp-8-6103-2008

Kam, H., Kim, Y. H., Mitchell, N. J., Kim, J. H., and Lee, C. (2019). Evaluation of estimated mesospheric temperatures from 11-year meteor radar datasets of King Sejong Station (62°S, 59°W) and Esrange (68°N, 21°E). *J. Atmos. Sol.-Terr. Phys.*, *196*, 105148. https://doi.org/10.1016/j.jastp.2019.105148

Kumar, K. K. (2007). Temperature profiles in the MLT region using radar–meteor trail decay times: Comparison with TIMED/SABER observations. *Geophys. Res. Lett.*, *34*(16), L16811. https://doi.org/10.1029/2007GL030704

Lee, C., Kim, J. H., Jee, G., Lee, W., Song, I. S., and Kim, Y. H. (2016). New method of estimating temperatures near the mesopause region using meteor radar observations. *Geophys. Res. Lett.*, *43*(20), 10580–10585. https://doi.org/10.1002/2016GL071082

Lee, C. S., Younger, J. P., Reid, I. M., Kim, Y. H., and Kim, J. H. (2013). The effect of recombination and attachment on meteor radar diffusion coefficient profiles. *J. Geophys. Res.: Atmos.*, *118*(7), 3037–3043. https://doi.org/10.1002/jgrd.50315

Liu, L. B., Liu, H. X., Chen, Y. D., Le, H. J., Sun, Y. Y., Ning, B. Q., Hu, L. H., and Wan, W. X. (2017a). Variations of the meteor echo heights at Beijing and Mohe, China. *J. Geophys. Res.: Space Phys.*, *121*(1), 1117–1127. https://doi.org/10.1002/2016JA023448

Liu, L. B., Liu, H. X., Le, H. J., Chen, Y. D., Sun, Y. Y., Ning, B. Q., Hu, L. H., Wan, W. X., Li, N., and Xiong, J. G. (2017b). Mesospheric temperatures estimated from the meteor radar observations at Mohe, China. *J. Geophys. Res.: Space Phys.*, *122*(2), 2249–2259. https://doi.org/10.1002/2016JA023776

Nguyen, V., and Palo, S. E. (2013). Technique to produce daily estimates of the migrating diurnal tide using TIMED/SABER and EOS Aura/MLS. *J. Atmos. Sol.-Terr. Phys.*, *105–106*, 39–53. https://doi.org/10.1016/j.jastp.2013.07.008

Nielsen, K. P., Röttger, J., and Sigernes, F. (2001). Simultaneous measurements of temperature in the upper mesosphere with an Ebert–Fastie spectrometer and a VHF meteor radar on Svalbard (78°N, 16°E). *Geophys. Res. Lett.*, *28*(5), 943–946. https://doi.org/10.1029/2000GL012357

Picone, J. M., Hedin, A. E., Drob, D. P., and Aikin, A. C. (2002). NRLMSISE-00 empirical model of the atmosphere: Statistical comparisons and scientific issues. *J. Geophys. Res.: Space Phys.*, *107*(A12), 1468. https://doi.org/10.1029/2002JA009430

Reid, I. M., Spargo, A. J., Woithe, J. M., Klekociuk, A. R., Younger, J. P., and Sivjee, G. G. (2017). Seasonal MLT-region nightglow intensities, temperatures, and emission heights at a Southern Hemisphere midlatitude site. *Ann. Geophys.*, *35*(3), 567–582. https://doi.org/10.5194/angeo-35-567-2017

Remsberg, E. E., Marshall, B. T., Garcia-Comas, M., Krueger, D., Lingenfelser, G. S., Martin-Torres, J., Mlynczak, M. G., Russell, J. M. III, Smith, A. K., … Thompson, R. E. (2008). Assessment of the quality of the Version 1.07 temperature-versus-pressure profiles of the middle atmosphere from TIMED/SABER. *J. Geophys. Res.: Atmos.*, *113*(D17), D17101. https://doi.org/10.1029/2008JD010013

Schwartz, M. J., Lambert, A., Manney, G. L., Read, W. G., Livesey, N. J., Froidevaux, L., Ao, C. O., Bernath, P. F., Boone, C. D., … Wu, D. L. (2008). Validation of the Aura Microwave Limb Sounder temperature and geopotential height measurements. *J. Geophys. Res.: Atmos.*, *113*(D15), D15S11. https://doi.org/10.1029/2007JD008783

Smith, A. K., Garcia, R. R., Moss, A. C., and Mitchell, N. J. (2017). The semiannual oscillation of the tropical zonal wind in the middle atmosphere derived

from satellite geopotential height retrievals. *J. Atmos. Sci.*, *74*(8), 2413–2425. https://doi.org/10.1175/JAS-D-17-0067.1

Stober, G., Jacobi, C., Matthias, V., Hoffmann, P., and Gerding, M. (2012). Neutral air density variations during strong planetary wave activity in the mesopause region derived from meteor radar observations. *J. Atmos. Sol.-Terr. Phys.*, *74*, 55–63. https://doi.org/10.1016/j.jastp.2011.10.007

Stober, G., Matthias, V., Brown, P., and Chau, J. L. (2014). Neutral density variation from specular meteor echo observations spanning one solar cycle. *Geophys. Res. Lett.*, *41*(19), 6919–6925. https://doi.org/10.1002/2014GL061273

Takahashi, H., Nakamura, T., Tsuda, T., Buriti, R. A., and Gobbi, D. (2002). First measurement of atmospheric density and pressure by meteor diffusion coefficient and airglow OH temperature in the mesopause region. *Geophys. Res. Lett.*, *29*(8), 6-1–6-4. https://doi.org/10.1029/2001GL014101

Tang, Y. H., Hao, X. J., Qiu, S. C., Cheng, W. H., Yang, C. Y., and Wu, J. F. (2023). Intraseasonal variation in the mesosphere observed by the Mengcheng meteor radar from 2015 to 2020. *Atmosphere*, *14*(6), 1034. https://doi.org/10.3390/atmos14061034

Xu, J. Y., She, C. Y., Yuan, W., Mertens, C., Mlynczak, M., and Russell, J. (2006). Comparison between the temperature measurements by TIMED/SABER and lidar in the midlatitude. *J. Geophys. Res.*: *Space Phys.*, *111*(A10), A10S09. https://doi.org/10.1029/2005JA011439

Yi, W., Chen, J. S., Ma, C. B., Li, N., and Zhao, Z. W. (2014). Observation of upper atmospheric temperature by Kunming all-sky meteor radar. *Chinese J. Geophys.*, *57*(5), 750–760. https://doi.org/10.1002/cjg2.20138

Yi, W., Xue, X. H., Chen, J. S., Dou, X. K., Chen, T. D., and Li, N. (2016). Estimation of mesopause temperatures at low latitudes using the Kunming meteor radar. *Radio Sci.*, *51*(3), 130–141. https://doi.org/10.1002/2015RS005722

Yi, W., Reid, I. M., Xue, X. H., Younger, J. P., Spargo, A. J., Murphy, D. J., Chen, T. D., and Dou, X. K. (2017). First observation of mesosphere response to the solar wind high-speed streams. *J. Geophys. Res.*: *Space Phys.*, *122*(8), 9080–9088. https://doi.org/10.1002/2017JA024446

Yi, W., Xue, X. H., Reid, I. M., Younger, J. P., Chen, J. S., Chen, T. D., and Li, N. (2018). Estimation of mesospheric densities at low latitudes using the Kunming meteor radar together with SABER temperatures. *J. Geophys. Res.*: *Space Phys.*, *123*(4), 3183–3195. https://doi.org/10.1002/2017JA025059

Yi, W., Xue, X. H., Chen, J. S., Chen, T. D., and Li, N. (2019a). Quasi-90-day oscillation observed in the MLT region at low latitudes from the Kunming meteor radar and SABER. *Earth Planet. Phys.*, *3*(2), 136–146. https://doi.org/10.26464/epp2019013

Yi, W., Xue, X. H., Reid, I. M., Murphy, D. J., Hall, C. M., Tsutsumi, M., Ning, B. Q., Li, G. Z., Vincent, R. A., … Dou, X. K. (2019b). Climatology of the mesopause relative density using a global distribution of meteor radars. *Atmos. Chem. Phys.*, *19*(11), 7567–7581. https://doi.org/10.5194/acp-19-7567-2019

Yi, W., Xue, X. H., Reid, I. M., Murphy, D. J., Hall, C. M., Tsutsumi, M., Ning, B. Q., Li, G. Z., Yang, G. T., … Dou, X. K. (2021). Climatology of interhemispheric mesopause temperatures using the high-latitude and middle-latitude meteor radars. *J. Geophys. Res.*: *Atmos.*, *126*(6), e2020JD034301. https://doi.org/10.1029/2020JD034301

Yi, W., Xue, X. H., Zeng, J., Wang, J. Y., Zhou, B. Z., Ye, H. L., Chen, T. D., and Dou, X. K. (2023). Observation of MLT region winds and tides by the USTC Mengcheng meteor radar. *JUSTC*, *53*(5), 0501. https://doi.org/10.52396/JUSTC-2022-0158

Younger, J. P., Lee, C. S., Reid, I. M., Vincent, R. A., Kim, Y. H., and Murphy, D. J. (2014). The effects of deionization processes on meteor radar diffusion coefficients below 90 km. *J. Geophys. Res.*: *Atmos.*, *119*(16), 10027–10043. https://doi.org/10.1002/2014JD021787

Younger, J. P., Reid, I. M., Vincent, R. A., and Murphy, D. J. (2015). A method for estimating the height of a mesospheric density level using meteor radar. *Geophys. Res. Lett.*, *42*(14), 6106–6111. https://doi.org/10.1002/2015GL065066

Zhou, B. Z., Xue, X. H., Yi, W., Ye, H. L., Zeng, J., Chen, J. S., Wu, J. F., Chen, T. D., and Dou, X. K. (2022). A comparison of MLT wind between meteor radar chain data and SD-WACCM results. *Earth Planet. Phys.*, *6*(5), 451–464. https://doi.org/10.26464/epp2022040

Zhou, B. Z., Yi, W., Xue, X. H., Ye, H. L., Zeng, J., Li, G. Z., Tsutsumi, M., Gulbrandsen, N., Chen, T. D., and Dou, X. K. (2023). Impact of sudden stratospheric warmings on the neutral density, temperature and wind in the MLT region. *Front. Astron. Space Sci.*, *10*, 1192985. https://doi.org/10.3389/fspas.2023.1192985